An International Journal
computers & mathematics
with applications

PERGAMON Computers and Mathematics with Applications 46 (2003) 719–739

www.elsevier.com/locate/camwa

A Numerical Study of Postshock Oscillations in Slowly Moving Shock Waves

Y. STIRIBA*
CERFACS/CFD Team, 42 Av. Gaspard Coriolis, 31057
Toulouse Cedex 1, France
youssef.stiriba@cerfacs.fr

R. DONAT†
Dept. de Matemática Aplicada, Universidad de Valencia
Dr. Moliner 50, 46100 Burjassot (Valencia), Spain
donat@uv.es

(Received May 2001; revised and accepted October 2002)

Abstract—Godunov-type methods and other shock capturing schemes can display pathological behavior in certain flow situations. This paper discusses the numerical anomaly associated to slowly moving shocks. We present a series of numerical experiments that illustrate the formation and propagation of this pathology, and allows us to establish some conclusions and question some previous conjectures for the source of the numerical noise. A simple diagnosis on an explicit Steger-Warming scheme shows that some intermediate states in the first time steps deviate from the true direction and contaminate the flow structure. A remedy is presented in the form of a new flux split method with an entropy intermediate state that dissipates the oscillations to a numerically acceptable level, and fix or reduce a variety of numerical pathologies.

Keywords—Nonlinear systems of conservation laws, Shock capturing schemes, Flux split methods, Slowly moving shocks, Compressible flows.

1. INTRODUCTION

The phenomenon of postshock oscillations in slowly moving shock waves is a numerical anomaly that has attracted much attention in recent times [1–6]. It has a significant importance in computational aeroacoustics [1], where the acoustic signals may be confused with the oscillations generated by quasi-stationary shock waves, and in transonic flow [6], where the convergence to steady state is very slow due to the oscillatory behavior displayed by upwind schemes.

The problem was first observed and discussed by Woodward and Colella [7]. They noted the existence of a source of numerical errors when using Godunov's method to compute an extremely strong shock moving slowly with respect to the grid. The dissipation in this method becomes very small across a slow shock, then insufficient to ensure a correct entropy production across the shock.

* Prsent address: IGPM, RWTH-AACHEN, Templergraben 55, D-52056 Aachen, Germany. E-mail: stiriba@igpm.rwth-aachen.de.

†The second author is supported in part by MYCT-BFM2001-2814.

0898-1221/03/$ - see front matter Typeset by AMS-TEX
doi: 10.1016/S0898-1221(03)00280-3

Roberts [6] showed that the same phenomenon occurs also for weak slow shocks. The error, which occurs only in systems of equations, consists of a long wavelength noise in the characteristics not belonging to the shock family, while the characteristics associated with the shock remain monotone. Different schemes seem to behave differently with respect to the level of noise—for example, Osher's scheme performed much better than Roe or Godunov's schemes [6]. Roberts focuses on the discrete shock structure to explain these differences and concludes that methods with numerical flux functions that recognize the Rankine-Hugoniot jump conditions (e.g., Godunov, Roe) may be less suitable for shock capturing than those using differentiable flux functions (e.g., Osher). He also observed that the use of total variation diminishing (TVD) concepts in high-order accurate methods accentuates this kind of problem.

After the work of Roberts, a number of authors have returned to the slowly-moving shock problem trying to understand the generation and propagation of these errors.

Jin and Liu [2] observe that at a slowly moving shock, a smeared density profile introduces a strong undershoot in the momentum profile at the shock location. They demonstrate the existence of the momentum spike using a traveling wave analysis on the viscous Euler equations, and show that it is nonphysical (it does not appear in solutions to the full Navier-Stokes equations). Their line of reasoning leads them to conclude that the unsteadiness in the momentum spike is the main cause of the postshock oscillations.

Arora and Roe [1] explained that numerical schemes in conservation form generate intermediate states that in turn produce a whole fan of waves, not only the shock wave itself, which are responsible for the generation of the errors. They found, in addition, that the magnitude of the errors is affected by the degree of nonlinearity[1]—the errors become small (large) as the nonlinearity decreases (increases). It is worth mentioning, in this same direction, that the amplitude of the oscillations depends on the direction of propagation of the shock—the maximum amplitude from low density to high density regions is bigger than that in the opposite direction (see [4]).

Karni and Canic [3] use some of the techniques developed in [1,6] to examine the different behavior exhibited by Roe's scheme and the Lax-Friedrichs (LxF) scheme. Focusing on the structure of the discrete shock profiles for many time steps, they are able to conclude that the lack of dissipation in Roe's scheme around a sign change in the eigenvalue corresponding to the shock family contributes to the generation of the oscillations. They use a modified equation analysis to illustrate the important role of higher-order terms in the local truncation error and to shed some light into the mechanism that projects the perturbation into all the characteristic families.

Based on all the aforementioned references and numerical observations, we analyze in this paper the behavior of several numerical schemes in conservation form. The paper is organized as follows. In Section 2, we use a well-known test problem on the Euler equations of gas dynamics to display the pathological behavior under observation for the schemes we consider. The behavior of the flux-vector splitting schemes is found to be different from that of the flux-difference splitting methods. In addition, we investigate the pathological behavior for some higher-order extensions of the basic first-order schemes considered and we find that, in contrast with the observation of Roberts in [6], in some cases the numerical anomaly is not accentuated. In Section 3, we look at the stability of the viscous shock profile and examine its relation with the downstream oscillations. Jin and Liu's conjecture on the source of the noise is questioned, following the observations from our numerical tests.

In Section 4, we switch to a simpler model, the isothermal Euler equations, and follow [3] to examine the numerical orbits in phase space in order to visualize the numerical evolution of internal shock structure of the different schemes with time.

[1]The nonlinearity of the systems of PDE is measured by the quantity [1]

$$\Delta = \frac{\lambda_L - \lambda_R}{s},$$

where s is the shock speed and λ_L and λ_R are the left and right wave speeds, respectively.

In Section 5.1, we present a simple diagnosis with the explicit Steger-Warming scheme. The *cure* to the problem that has invariably been proposed in all the aforementioned works consists of adding a *judicious* (problem dependent) amount of numerical dissipation. In Section 5.2, we present a remedy in the form of a flux split method with an entropy intermediate state that leads to a higher-order scheme with an oscillation free density profile. Some examples of our modified numerical scheme for the Euler equations are presented. The results show that our method can handle complex situations remarkably well.

Finally, we end this study with a summary and some concluding remarks.

2. THE NUMERICAL SIMULATION OF SLOWLY MOVING SHOCK WAVES

Colella and Woodward [7] define a slow shock as one that moves slowly with respect to the grid, i.e., it takes many time steps to cross one computational cell,

$$\frac{s}{\lambda_{\max}} \ll 1, \tag{1}$$

where s is the shock speed and $\lambda_{\max}$ is the maximum wave speed in the domain. Since for stationary shocks there is a sign change in the shock characteristic across the shock front, this will also be the case for shocks that move sufficiently slowly, a characterization [1,3,6] that relates the casuistics of a slow shock to the nonlinearity of the system, and that will be particularly relevant to our discussion.

We shall display the numerical pathology associated to the computation of slowly-moving shocks in the 1-D Euler equations for an ideal gas

$$q_t + f(q)_x = 0, \tag{2}$$

where

$$q = \begin{pmatrix} \rho \\ m \\ E \end{pmatrix} \quad \text{and} \quad f(q) = \begin{pmatrix} m \\ \rho u^2 + p \\ u(E+p) \end{pmatrix}. \tag{3}$$

Here ρ is the density, u the velocity, $m = \rho u$ the momentum, and E is total energy. For a polytropic gas, the equation of state is given by

$$p = (\gamma - 1)\left(E - \frac{1}{2}\rho u^2\right), \tag{4}$$

where $\gamma = c_v/c_p = 1.4$ is the ratio of specific heats. The initial data we consider in our first set of computations corresponds to a Mach 3 shock moving to the right with a speed $s = 0.1096$ [2,5]

$$q_L = \begin{pmatrix} 3.86 \\ -3.1266 \\ 27.0913 \end{pmatrix}, \quad \text{if } 0 < x < 0.1; \qquad q_R = \begin{pmatrix} 1 \\ -3.44 \\ 8.4168 \end{pmatrix}, \quad \text{if } 0.1 \le x < 1. \tag{5}$$

The behavior of various flux-difference splitting schemes has been examined in several papers [1–3,6]. Here we consider five different examples of numerical flux functions for the numerical experiments: Lax-Friedrichs (LxF), Steger-Warming (SW) [8], van Leer (VL) [9] as representatives of the classical flux-vector splitting (FVS) methods, the Roe's scheme [10] as a representative of the flux-difference splitting (FDS) methods, and the newer Marquina's flux split method [11].

In [1–3,6,11] it is observed that the numerical computation of slowly-moving shock waves always displays an anomalous behavior, which is inherent to nonlinear systems: the numerical values in the postshock region display an oscillatory behavior which is completely nonphysical.

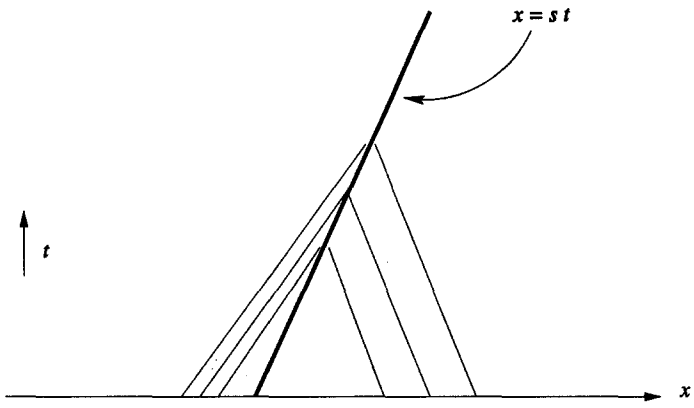

Figure 1. A slow shock.

Numerical results for the density of the Euler equations, computed by first-order schemes, are displayed in Figure 2. The solutions displayed correspond to 160 and 4000 time steps with $\Delta x = 0.01$, $\Delta t/\Delta x = 0.1$. We clearly observe the presence of a long wavelength error in the postshock region. At this stage the solution changes from an artificially narrow to a continuous profile, which is a large perturbation of the viscous profile. These errors are generated at the beginning of the computation in *all* schemes. The numerically generated noise travels left with speed $u_L - c_L$ where c_L is the speed of sound. While the generation of the numerical postshock errors is common to all the schemes reported in the literature, it is worth noticing the different behavior exhibited by the different schemes at later times. While the start-up errors seem to be continuously generated in time *with the same amplitude* in Roe's scheme, in all the FVS schemes considered here the amplitude of the noise diminishes with time; i.e., the numerical noise is being damped by the numerical viscosity present in the scheme.

In the LxF scheme, the noise at time $t = 4$ is undetectable. The original perturbation travels left with speed $u_L - c_L$, and when it abandons the computational domain through the left boundary leaves an oscillation-free numerical shock profile. The behavior of VL and SW with respect to the damping of the noise is quite similar, leading us to believe that their damping mechanism should be also quite similar, but the shock profile in VL's scheme is sharper. On the other hand, Marquina's scheme seems to suffer 'barely detectable' postshock oscillations at time $t = 4$ (the error in the numerical approximation obtained with Roe's scheme is close to 10%, and with Marquina's scheme around 1% at $t = 4$).

It has been observed in [1–3,6] that this pathological behavior worsens when using higher-order versions of a numerical scheme. The standard explanation is that the numerical viscosity in a higher-order scheme is less than that of the corresponding first-order scheme, and thus the effects derived from the lack of viscosity are accentuated.

The numerical noise associated to slowly-moving shock computations is usually linked to the lack of sufficient dissipation in the numerical scheme. In a higher-order scheme, in which the numerical viscosity supplied by the scheme is reduced, the pathological behavior is most likely to be accentuated, since the damping process due to the numerical viscosity of the scheme is also reduced.

The first column of Figure 3 displays the numerical shock profiles for the density of a second-order extension of each one of the numerical schemes we consider. This extension has been designed using an ENO-2 piecewise polynomial reconstruction technique applied to the numerical flux function, as specified in [12]. The numerical results shown here are consistent with those of Roberts [6] and Jin and Liu [2]: the noise is preserved for longer distances downstream. These results, however, should be compared with the numerical shock profiles displayed in the second column of the same figure. In this case, we have employed the piecewise hyperbolic method (PHM) of [13] in the reconstruction process, which leads to (formally) third-order accurate numerical

schemes. It can be clearly appreciated that the postshock oscillations are never worse than those in the second-order extension of the same scheme. In some cases, for example in Roe's scheme, their amplitude is noticeably smaller and the damping upstream is more effective. The fact that the PHM reconstruction seems to be more robust in some particular situations was already observed in [11], where a significant difference between the ENO-3 and PHM high resolution versions of Marquina's scheme were compared in a slowly moving shock computation. Although both schemes are formally third-order accurate, the downstream noise obtained with piecewise polynomial-based extensions ENO-3 was larger (and preserved further upstream) than that of the PHM-based extension, presumably because the latter is more local and requires only four points to reconstruct a piecewise smooth function, in contrast to ENO-3 that uses six points.

The numerical experiments we have reported here show that the combination of numerical flux function/higher-order reconstruction technique plays an important role in the behavior of the numerical oscillations with time; in particular, it is not true that the use of TVD/ENO concepts in constructing higher-order schemes from basic first-order ones has to necessarily lead to a numerical solution in which the anomalous behavior is amplified and/or further preserved in the downstream region.

REMARK 1. The "overheating effects" generated by shock capturing schemes in shock reflection problems [14] are another numerical pathology with a similar behavior. It appears in the first time steps and may persist for all time, depending on the damping mechanism of the numerical scheme.

3. THE NUMERICAL PROFILE OF SLOWLY MOVING SHOCKS

Jin and Liu [2] observe that in slowly-moving shock computations the momentum profile will develop a numerical artifact: an unphysical peak, which is responsible for the generation of the errors. The viscosity terms present in any numerical scheme, together with the small shock speed, are the cause of the peak, which generates diffusion waves to balance momentum conservation. According to Jin and Liu, the unsteady nature of the momentum profile, and in particular of the momentum spike, is a constant source of new downstream errors.

It seems clear that the peak will perturb the viscous profile due to momentum conservation, but the connection between the unsteady nature of the momentum spike and the postshock oscillations deserves further examination.

In Figure 4, we display the time evolution of the momentum spike obtained with the first-order schemes we have considered. The plot corresponding to Roe's scheme can also be found in [2], where we observe that the analogous display for the LxF scheme (not shown here) shows that the momentum spike has an almost-steady nature. This fact is used by Jin and Liu to explain the lack of oscillations in the LxF scheme. However, the VL scheme has a perturbed viscous profile for all time, but the downstream errors become negligible after some time steps (compare Figures 2d′ and 4c). The same happens with all the other schemes considered, which seems to support the fact that the unsteady of the peak may contribute to the oscillations but there is no direct relation between the unsteady nature of the momentum profile and the postshock errors. We call the attention of the reader to Figures 8 and 9, where we consider an 'entropy-fix' type of cure for the oscillations. The proposed scheme has an oscillation free shock profile, even for the PHM higher-order extension, but the momentum spike displays an oscillatory behavior of the same nature (and amplitude) as in Roe's scheme.

A graphical display of the evolution of the momentum peak in the higher-order extensions of the schemes considered in this paper can be found in [15].

4. THE DISCRETE SHOCK CURVE: NUMERICAL ORBITS

The analysis of Jin and Liu leads to an interpretation of the phenomenon in the context of traveling wave solutions for the modified equations. These arguments were used in [3] to get a

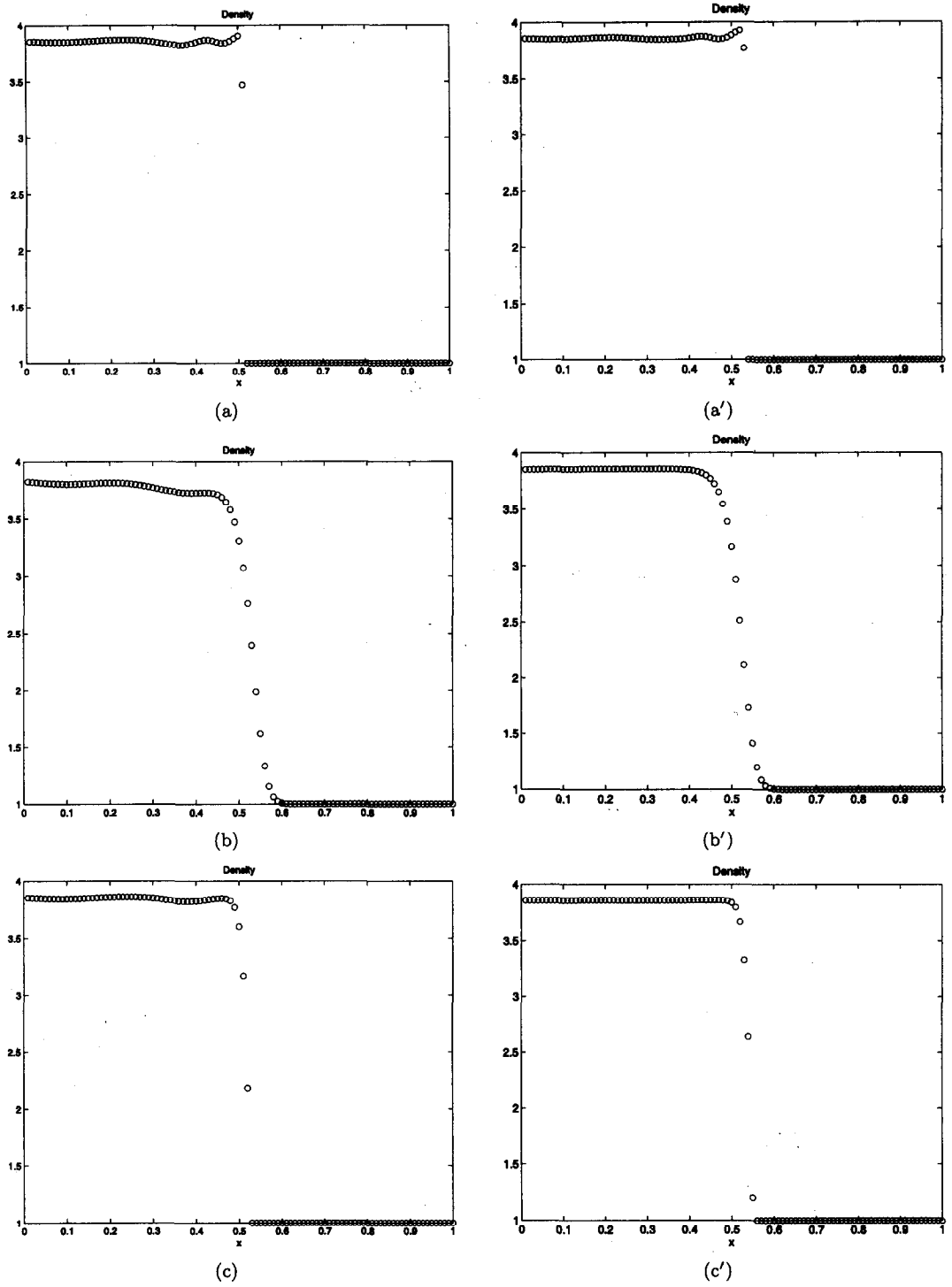

Figure 2. Density plots of a slowly moving shock at time $T = 0.16$ (left), $T = 4$ (right), computed by: (a)-(a′) Roe, (b)-(b′) Lax-Friedrichs, (c)-(c′) Steger-Warming, (d)-(d′) van Leer, and (e)-(e′) Marquina.

deep insight into the mechanism which might be responsible for the continuous generation of the postshock noise in Roe's scheme.

In what follows, we analyze the different schemes considered using the tools proposed in [1,3,6], namely numerical orbits in phase space diagrams. For this, we switch to a simpler model: the

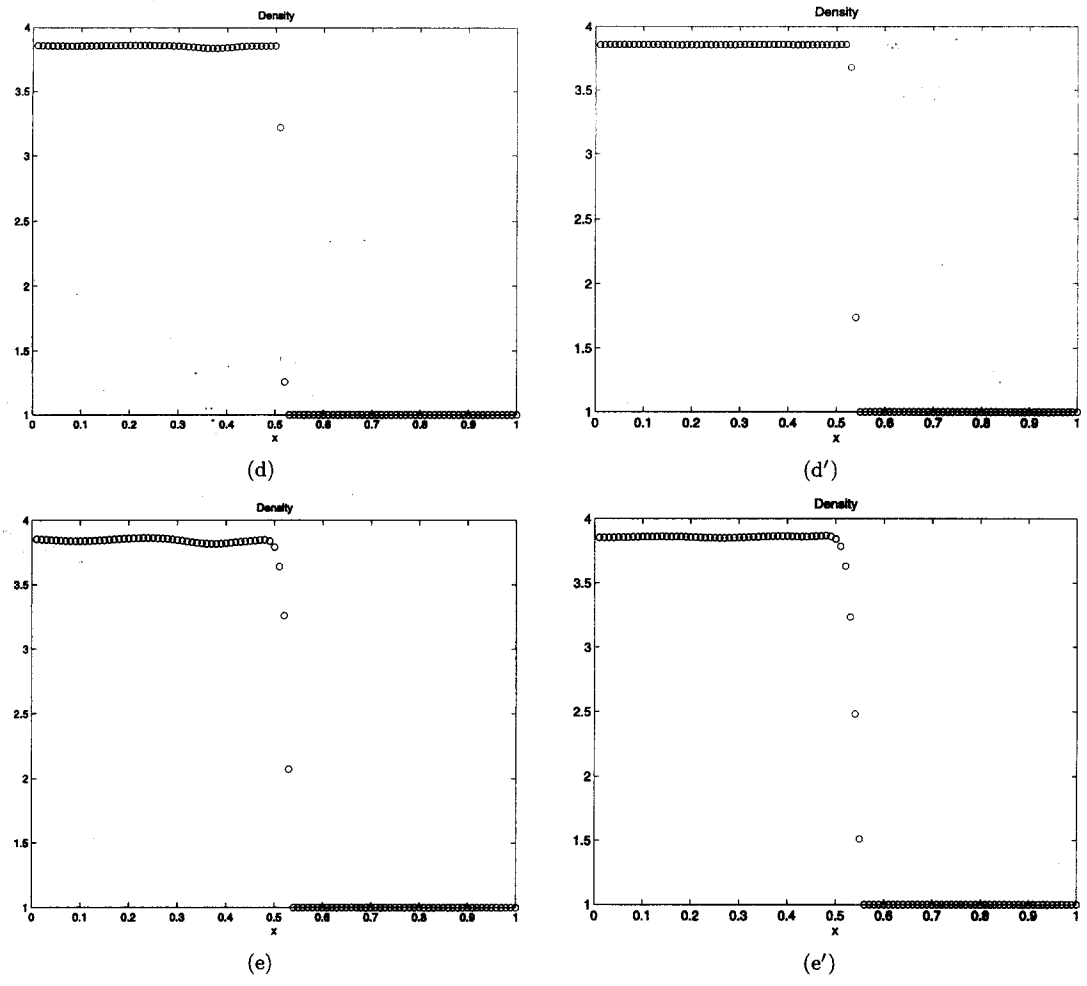

Figure 2. (cont.)

isothermal Euler equations, which take form (2), with

$$q = \begin{pmatrix} \rho \\ m \end{pmatrix} \qquad \text{and} \qquad f(q) = \begin{pmatrix} m \\ \rho u^2 + \rho c^2 \end{pmatrix}. \tag{6}$$

The initial data for the Riemann problem in this set of numerical experiments corresponds to two constants states separated by a discontinuity propagating slowly to the right with speed s (see [3])

$$q_L = \begin{pmatrix} 4 \\ 4s - 2 \end{pmatrix}, \quad \text{if } 0 \le x \le 0.5, \qquad q_R = \begin{pmatrix} 1 \\ s - 2 \end{pmatrix}, \quad \text{if } 0.5 \le x \le 1. \tag{7}$$

The constant c is taken to be 1.

As observed in [3], phase diagrams of computed propagating shocks yield extremely clean and well-defined numerical orbits as soon as the shocks settle into their viscous profile. The work in [3] supports the fact that these numerical orbits might represent traveling wave solutions of the *modified equations*. It is noticed in [3] that these modified equations should take into account higher-order terms in certain situations, when the leading-order terms in the local truncation error become too small.

According to Roberts [6] and Arora and Roe [1], the location of the intermediate states with respect to the Hugoniot locus is important. If these intermediate states were located exactly

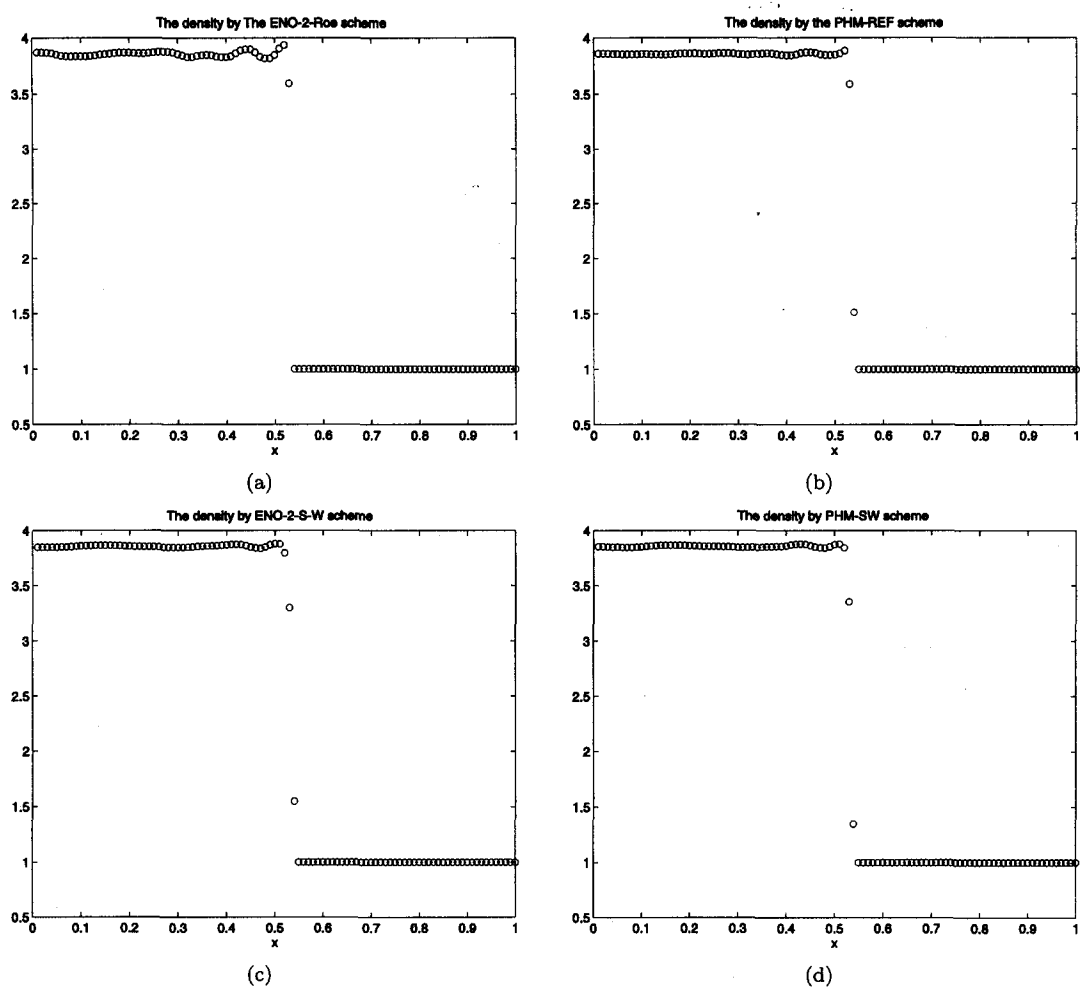

Figure 3. Density plots of a slowly moving shock at time $T = 4$ computed by: (a) ENO2-R, (c) ENO2-SW, (e) ENO2-VL, (g) ENO2-M, (b) PHM-R, (d) PHM-SW, (f) PHM-VL, and (h) PHM-M.

in the Hugoniot locus, there would be no downstream waves. For this reason, we also plot the Hugoniot locus together with the numerical orbit.

We collect the data of the discrete shock profiles at each time step to plot them using (density, momentum) as coordinates in contrast to the work of Arora and Roe [1] which make use of the characteristic variables. It might be possible to use the numerical orbits to examine the numerical viscosity and compare it with the traveling wave solution. Such analysis is not a simple task due to the nonlinearity of the schemes and the difficulty to find their viscosity matrix. In Figures 5 and 6, we display the numerical orbits corresponding to the various schemes we consider in this paper. The first column in each figure collects the data obtained in the first stages of the computation, when the viscous-like profile is artificially narrow and is not well established yet. We have found it interesting to follow the location of path of these intermediate points toward the stable viscous-like profile. For the LxF, and scheme, each 'branch' of points moves smoothly towards the final profile. The same seems to happen for Marquina's scheme, although the final profile has a particularly 'kinky' behavior.

It is readily seen that the oscillatory tail projects onto the eigenvector $R_1(q_L)$ in all the schemes. The behavior of the numerical orbits for $t < 0.15$ and $t > 1.5$ is quite different in all schemes *except* in Roe's scheme, where the behavior is more or less the same. Another interesting feature is that the numerical orbit crosses the Hugoniot locus *only* for this particular scheme.

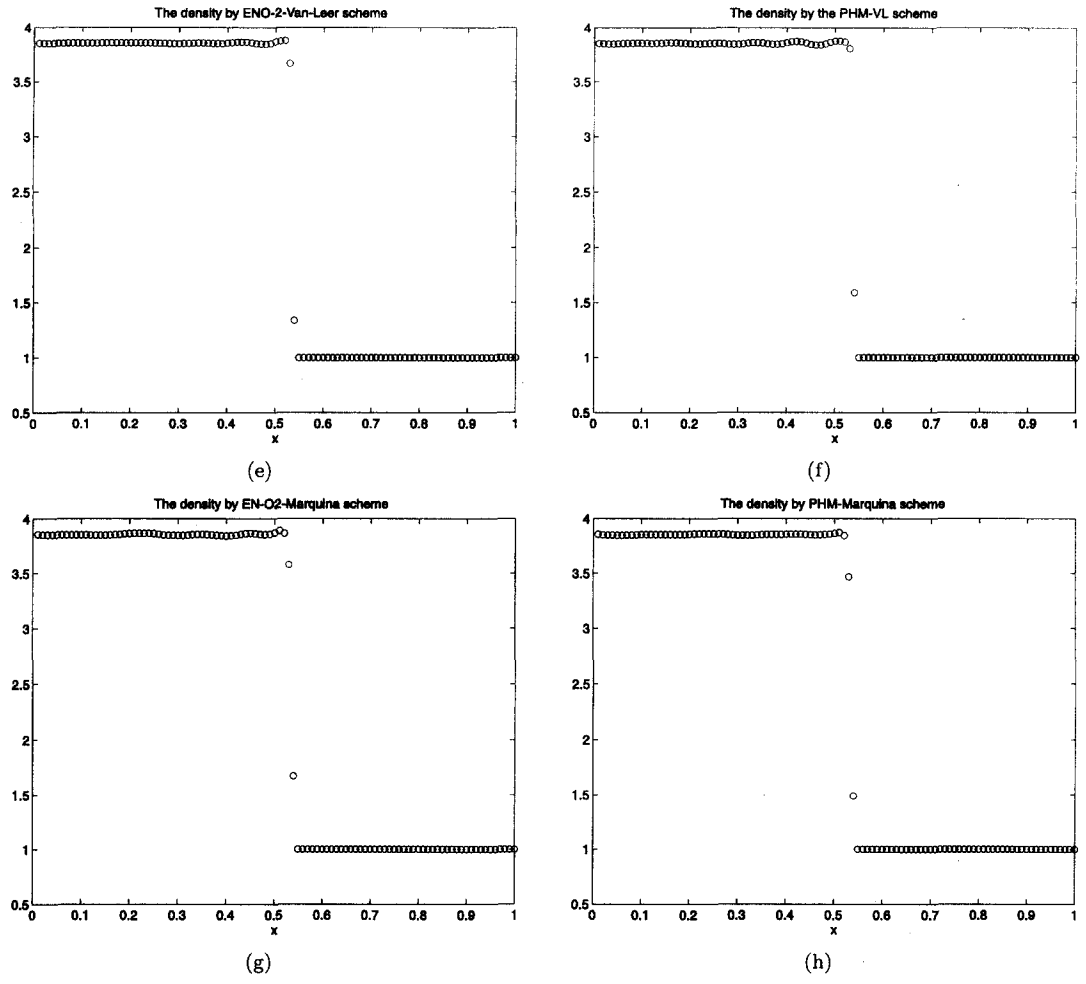

Figure 3. (cont.)

In addition, it is not clear at all that there is a link between the absence of oscillations and the 'closeness' of the numerical orbit to the Hugoniot locus, or the smoothness of the numerical orbit. For example, the LLF scheme described in [15] has a piecewise smooth numerical orbit with a well-defined discontinuity in derivative [15]; it is not particularly close to the Hugoniot locus, and it displays no oscillatory behavior for large time. The same thing happens for the VL scheme, although the numerical orbit seems to be smooth in this case. The numerical orbit is closer to the Hugoniot locus for the LF scheme, except in the middle region, and there are no noticeable oscillations in this case either.

5. AN ENTROPY FIX

5.1. A Diagnosis with Explicit Steger-Warming Scheme

What we have observed in our study of the numerical orbits is that there is always numerical noise in the first time steps, so the first internal zones deviate from the Hugoniot curve and generate a set of waves in other characteristic fields. Let us examine this fact by considering the system of the isothermal Euler equations and a simple flux function like SW-FVS.

Assume that we have a subsonic flow to the right (i.e., the left state is subsonic to the right, $|u_L/c| < 1$); see Figure 7.

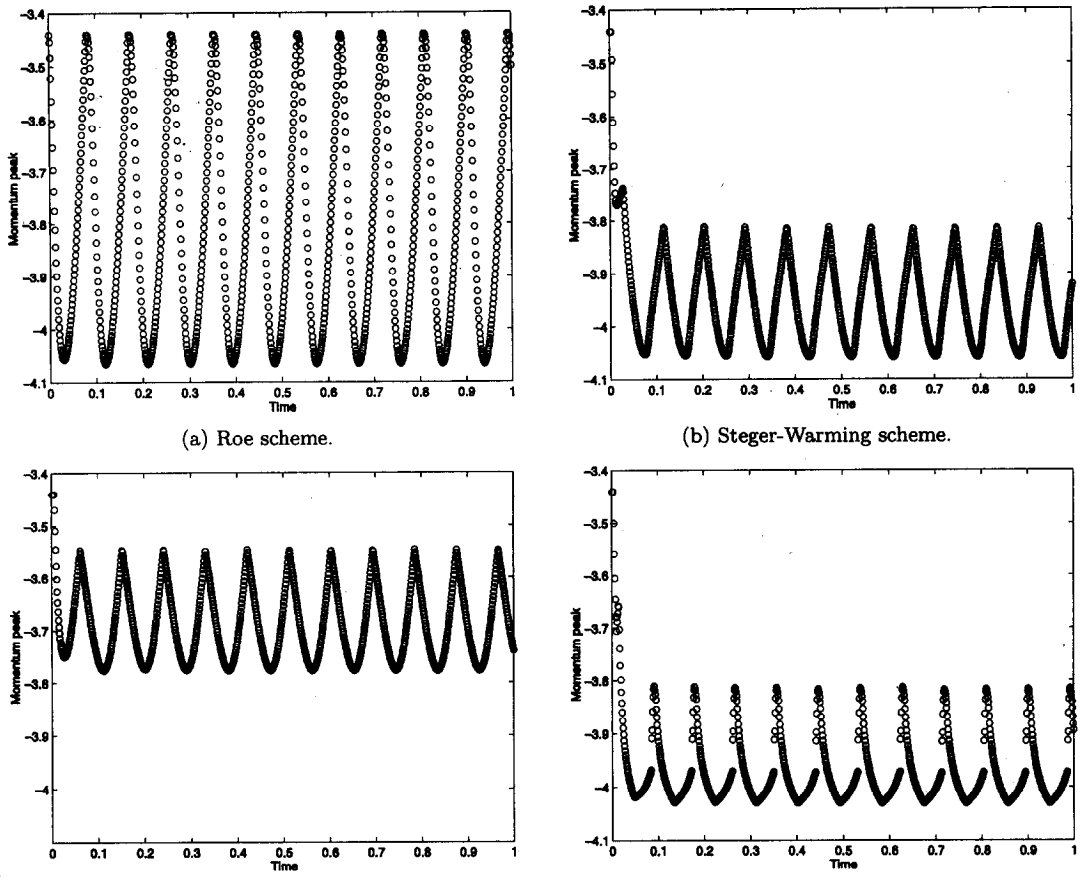

(a) Roe scheme.

(b) Steger-Warming scheme.

(c) Van Leer scheme.

(d) Marquina scheme.

Figure 4. Time evolution of the momentum spike.

Consider one time step of SW-FVS scheme

$$Q_i^{n+1} = Q_i^n - \frac{\Delta t}{\Delta x}\left(F_{i+1/2}^n - F_{i-1/2}^n\right). \tag{8}$$

The interface flux function between Q_i^n and Q_{i+1}^n is given by

$$\begin{aligned} F_{i+1/2}^n &= F\left(Q_{i+1}^n, Q_i^n\right) \\ &= f^+\left(Q_i^n\right) + f^-\left(Q_{i+1}^n\right) \\ &= \sum_{k=1}^{2}\left(\lambda_k^+\left(Q_i^n\right)\alpha^k\left(Q_i^n\right)R^k\left(Q_i^n\right) + \lambda_k^-\left(Q_{i+1}^n\right)\alpha^k\left(Q_{i+1}^n\right)R^k\left(Q_{i+1}^n\right)\right), \end{aligned}$$

where $\alpha^{1,2}$ are the characteristic variables such that

$$\alpha^1\left(Q_i^n\right) = L^1\left(Q_i^n\right).Q_i^n \qquad \text{and} \qquad \alpha^2\left(Q_i^n\right) = L^2\left(Q_i^n\right).Q_i^n. \tag{9}$$

For a slow shock (in our case a two-shock) subsonic to the right, we have

$$F_{i+1/2}^n = \lambda_2\left(Q_i^n\right)\alpha^2\left(Q_i^n\right)R^2\left(Q_i^n\right) + \sum_{k=1}^{2}\lambda_k\left(Q_{i+1}^n\right)\alpha^k\left(Q_{i+1}^n\right)R^k\left(Q_{i+1}^n\right). \tag{10}$$

Note that in our numerical experiments we have

$$q_L = \begin{pmatrix} 4 & 4s-2 \end{pmatrix}^\top, \qquad q_R = \begin{pmatrix} 1 & s-2 \end{pmatrix}^\top,$$

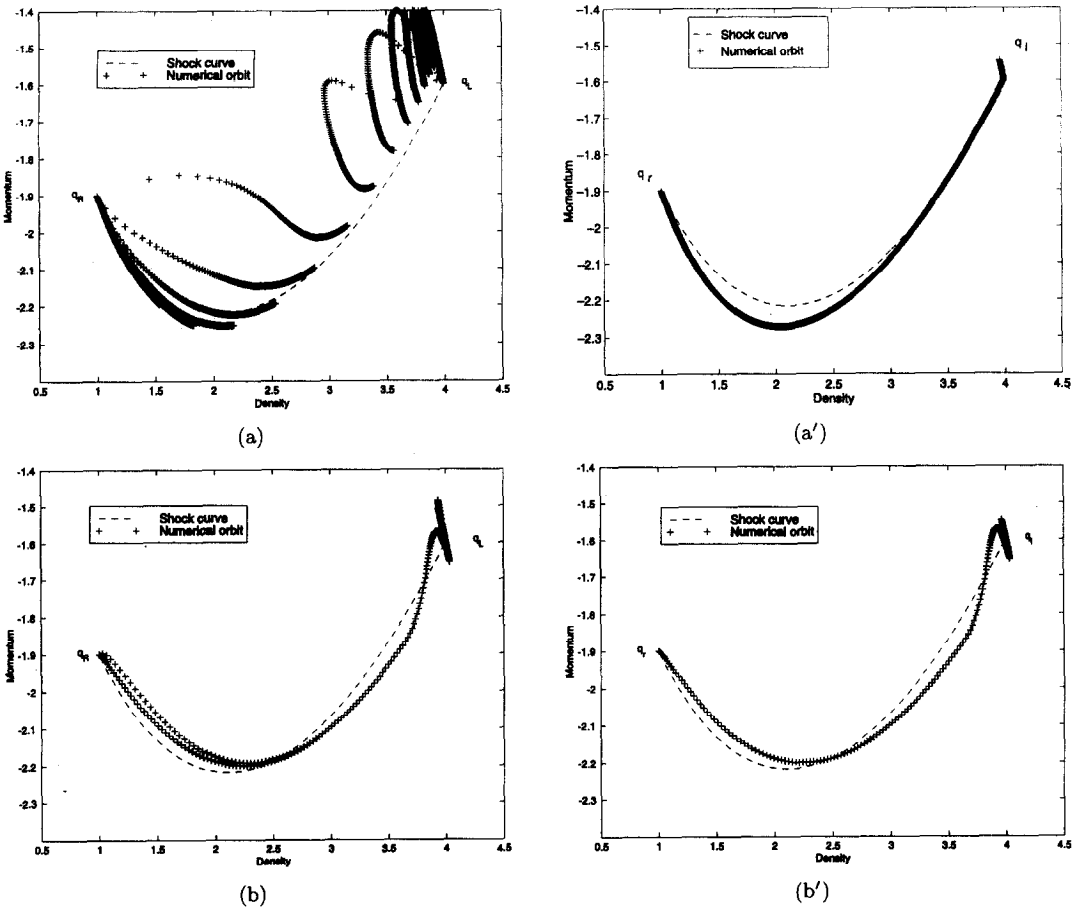

Figure 5. Shock curve and numerical orbit of a slow shock ($S = 0.1$), by (a)-(a′) Lax-Friedrichs and (b)-(b′) Roe, for time $t \in [0, 1.5]$ (left) and $t \geq 1.5$ (right).

so

$$\lambda_L^1 = u_L - c = s - 1.5, \qquad \lambda_R^1 = u_R - c = s - 3,$$

$$\lambda_L^2 = u_L + c = s + 0.5, \qquad \lambda_R^2 = u_R + c = s - 1.$$

For $s \ll 1$, we have postshock oscillations, but for $s > 3$ we are in a fast shock. Then for slow shock

$$\lambda_L^1 < 0, \qquad \lambda_R^1 < 0,$$

$$\lambda_L^2 > 0, \qquad \lambda_R^2 < 0.$$

Thus,

$$F_{i+1/2}^n = \lambda_2 \left(Q_i^n\right) \alpha^2 \left(Q_i^n\right) R^2 \left(Q_i^n\right) + f_{i+1}^n,$$

and

$$F_{i-1/2}^n = F\left(Q_i^n, Q_{i-1}^n\right) = F\left(Q_i^n, Q_i^n\right) = f_i^n$$

from consistency, where $f_i^n = f(q(i\Delta x, n\Delta t))$, $\forall i, n$. Then

$$\begin{aligned} Q_i^{n+1} - Q_i^n &= -\frac{\Delta t}{\Delta x}\left(F_{i+1/2}^n - F_{i-1/2}^n\right) \\ &= -\frac{\Delta t}{\Delta x}\left(\lambda_2 \left(Q_i^n\right) \alpha^2 \left(Q_i^n\right) R^2 \left(Q_i^n\right) + f_{i+1}^n - f_i^n\right) \end{aligned}$$

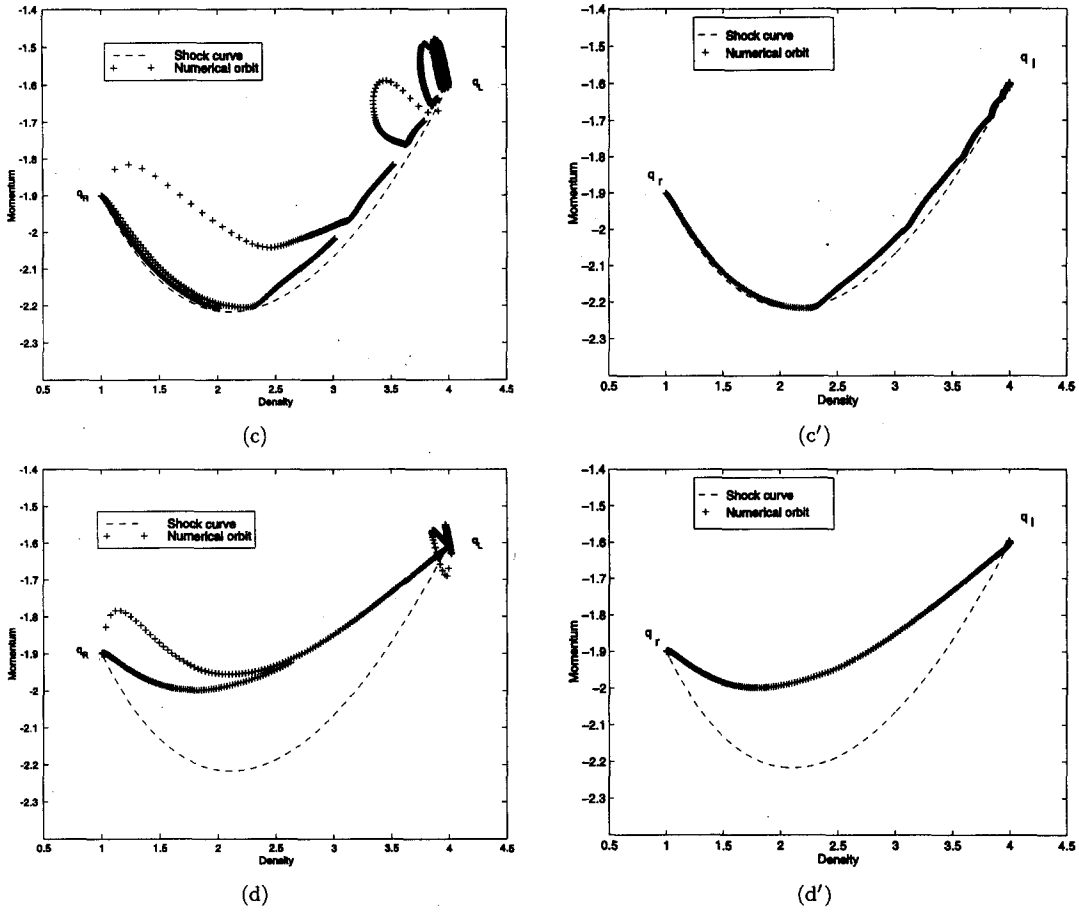

Figure 6. Shock curve and numerical orbit of a slow shock ($S = 0.1$), by (c)-(c') Steger-Warming, (d)-(d') van Leer, and (e)-(e') Marquina, for time $t \in [0, 1.5]$ (left) and $t \geq 1.5$ (right).

from R-H jump condition

$$\begin{aligned} &= -\frac{\Delta t}{\Delta x}\left(\lambda_2\left(Q_i^n\right)\alpha^2\left(Q_i^n\right)R^2\left(Q_i^n\right) + s\left(Q_{i+1}^n - Q_i^n\right)\right) \\ &= -\frac{\Delta t}{\Delta x}\left(-s\alpha^1\left(Q_i^n\right)R^1\left(Q_i^n\right)\right. \\ &\quad + \left(\lambda_2\left(Q_i^n\right) - s\right)\alpha^2\left(Q_i^n\right)R^2\left(Q_i^n\right) \\ &\quad \left. + s\left(\alpha^1\left(Q_{i+1}^n\right)R^1\left(Q_{i+1}^n\right) + \alpha^2\left(Q_{i+1}^n\right)R^2\left(Q_{i+1}^n\right)\right)\right). \end{aligned}$$

If there are no waves that go left leftward, we have

$$Q_i^{n+1} - Q_i^n = Q_i^{n+1} - Q_L \quad \alpha \quad R^2.$$

In a slow shock, $s = O(\epsilon)$, where ϵ is small enough, and $\Delta Q_i = Q_i^{n+1} - Q_i^n$ decouples into the direction of R^1 and R^2. The intermediate state deviates from the true direction and this implies generation of other waves in the other characteristic family.

Note that for a very slow shock, i.e., $s = o(\epsilon)$,

$$\Delta Q_i^n \to -\frac{\Delta t}{\Delta x}\lambda_2\left(Q_i^n\right)\alpha^2\left(Q_i^n\right)R^2\left(Q_i^n\right),$$

then, the intermediate zone approaches the Hugoniot curve. This is consistent with Lin's numerical observation [4], i.e., for a very slow shock the amplitude of oscillations is very small, since no leftward waves are generated.

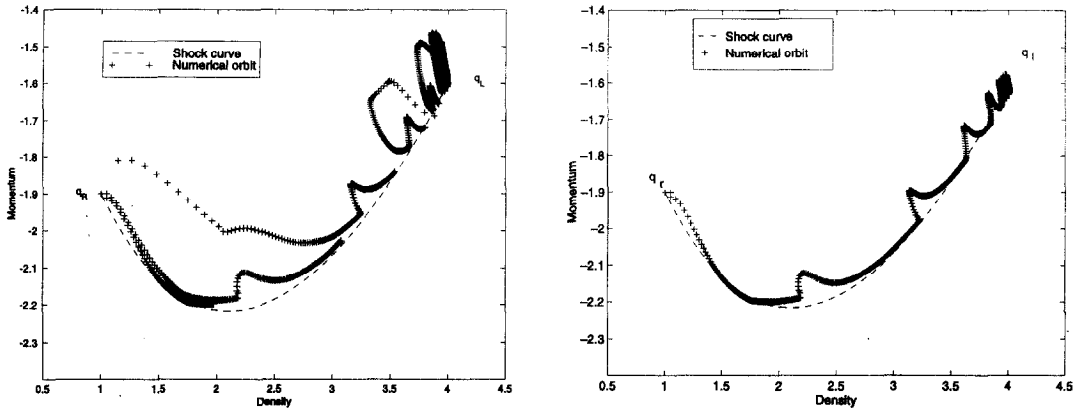

(e) (e′)

Figure 6. (cont.)

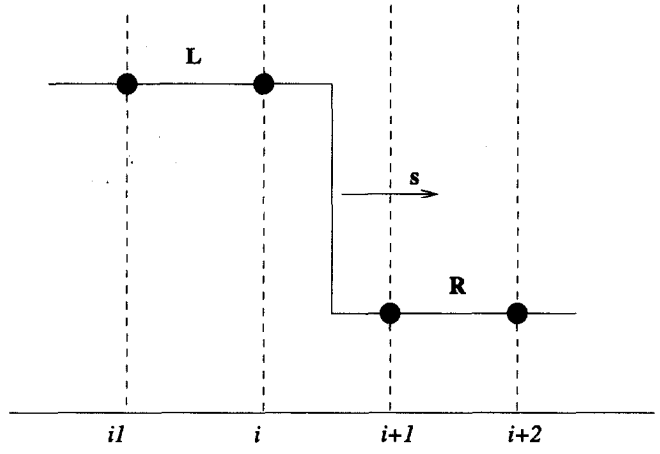

Figure 7. Shock structure inside a grid cell at time $t_n = n\Delta t$.

What happens in the case of fast shock?

In this case,

$$F^n_{i-1/2} = f^n_i, \qquad F^n_{i+1/2} = f^n_i, \qquad F^n_{i+3/2} = f^n_{i+1},$$

since $\lambda_L, \lambda_R > 0$. Then

$$Q^{n+1}_{i-1} = Q^n_{i-1}, \qquad Q^{n+1}_i = Q^n_i,$$

and

$$\begin{aligned} Q^{n+1}_{i+1} - Q^n_{i+1} &= -\frac{\Delta t}{\Delta x}\left(f^n_{i+1} - f^n_i\right) \\ &= -\frac{\Delta t}{\Delta x}\, s\left(Q^n_{i+1} - Q^n_i\right); \end{aligned}$$

i.e., Q^{n+1}_{i+1} is a new state that takes the direction of the straight line (Q_L, Q_R), called the projection P (see [1]). Our experiments confirm that for a fast shock the curve H tends to coincide with P, so no leftward waves are generated.

From this diagnosis, it appears that the one-off start-up errors appear at earlier time due to nonphysical intermediate states that deviate from the true direction, project on all characteristic fields, and give new downstream waves that contaminate the shock profile. We believe that, in addition, the momentum peak that appears in the first steps accentuates the problem and gives what we observed in Section 2. At later time steps, once the viscous profile is formed, the errors

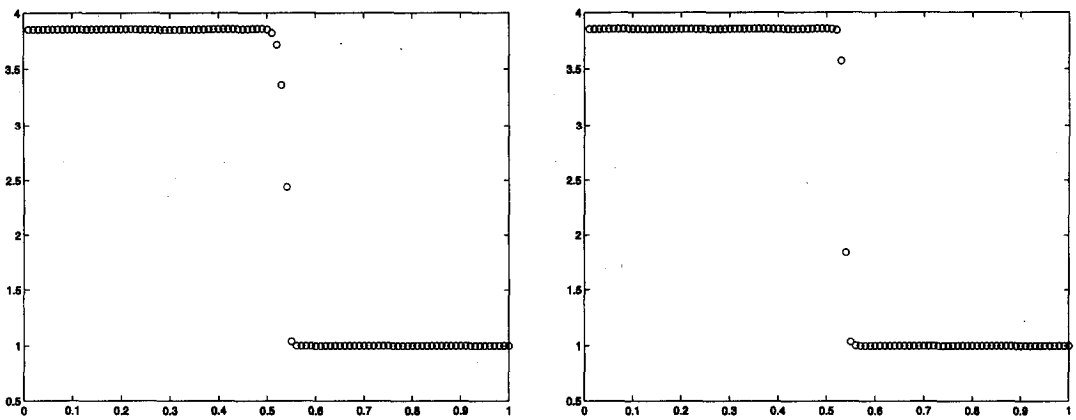

(a) First-order scheme. (b) Third-order hyperbolic scheme.

Figure 8. Density and pressure plots of a slowly moving shock at time $T = 4$.

seem to be continuously generated as wavy tail for some schemes, while the shock profile appears to be less oscillatory for other approaches by the numerical viscosity present in these schemes.

REMARK 2. Note that we only presented the analysis on the isothermal equations; the above study can be extended to the full Euler equations. For simplicity we only discuss the isothermal Euler equations, and numerical difficulties that do arise can be easily isolated and understood, yielding useful insight for the Euler equations.

5.2. A Dissipative Scheme

For a slow shock, all the schemes take many time steps to cross one computational cell and use both right and left informations many time steps near sonic points (when $\lambda_L.\lambda_R < 0$). In the neighborhood of a sonic point, the SW scheme has a noncontinuous transition in such field, while VL-FVS has a smooth transition, and Marquina switches to the local Lax-Friedrichs scheme [12]. Thus, the first intermediate states deviate from the true direction in a different manner for each scheme (Figures 8 and 9). This has been observed early in numerical orbits. The smoothness of such path is very important; we believe that this indicates that the scheme has additional artificial viscosity to damp out the oscillations with time.

It is well known that the SW scheme does not give good resolution near sonic points, since the splitting does not behave continuously as the Mach number passes through 1. Hence, we intend to add an intermediate state in the neighborhood of sonic points, using the transformation to local characteristic fields and the left and right sides of each cell wall, to produce a continuous transition. An entropy intermediate state Q^* between Q_i and Q_{i+1} always exists from the integral form of the conservation laws [16] over the control volume $(x_{i-1/2}, x_{i+1/2}) \times [t_n, t_{n+1}]$

$$Q^* = \frac{\lambda_R Q_{i+1} - \lambda_L Q_i - f(Q_{i+1}) + f(Q_i)}{\lambda_R - \lambda_L}. \tag{11}$$

Here $\lambda_L = \lambda(Q_i)$ and $\lambda_R = \lambda(Q_{i+1})$. The corresponding numerical flux is given by integrating (1) over the control volume $[x_{i-1/2}, x_i] \times [t_n, t_{n+1}]$ and using (11)

$$F(Q_i, Q_{i+1}) = \frac{\lambda_R(f(Q_i) - \lambda_L Q_i)}{\lambda_R - \lambda_L} + \frac{\lambda_L(-f(Q_{i+1}) + \lambda_R Q_{i+1})}{\lambda_R - \lambda_L}. \tag{12}$$

The new flux is computed as follows.

Consider a cell wall, $x_{i+1/2}$, where we have to evaluate the numerical flux function $F^n_{i+1/2}$, at a given time step n.

(1) Decompose the left state Q_i, the right state Q_{i+1}, and the flux function evaluated at these states into characteristic variables

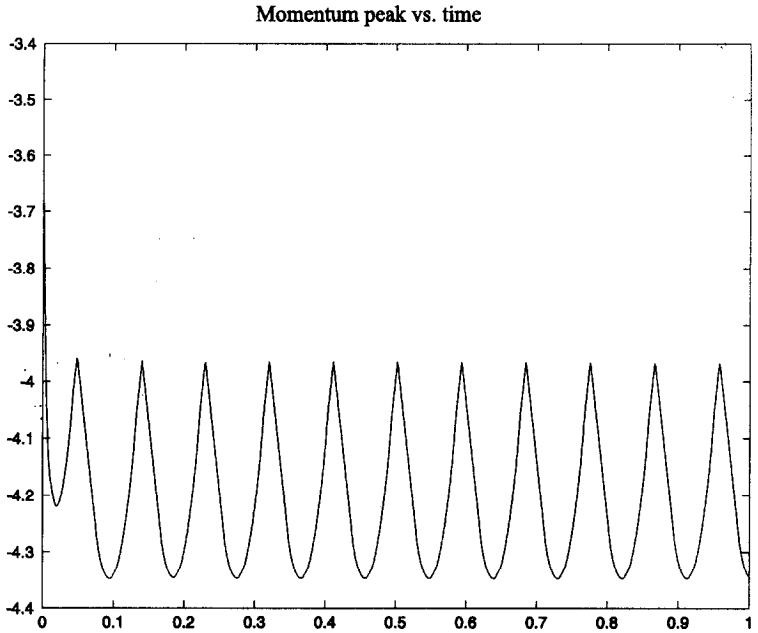

Figure 9. Momentum peak value vs. time by the flux split method combined with hyperbolic reconstruction.

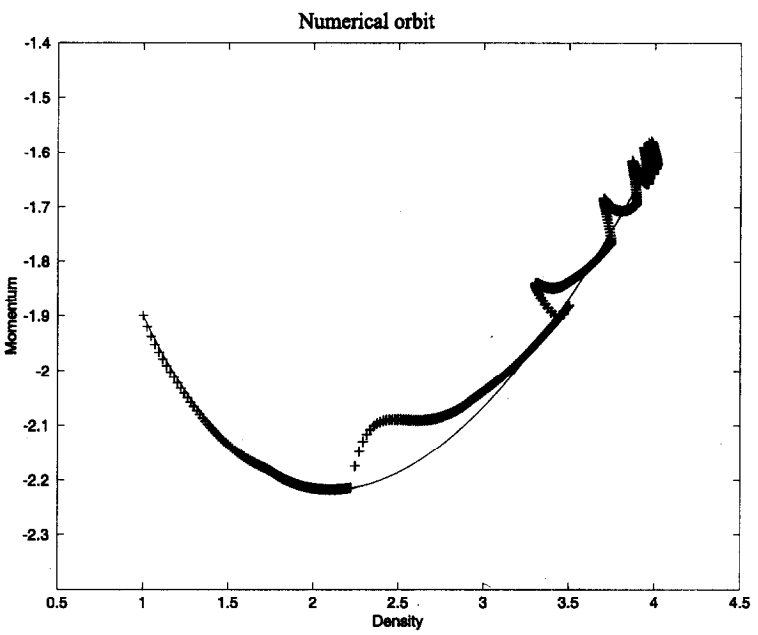

Figure 10. Shock curve and numerical orbit by the flux split method.

$$\omega_i^p = L^p(Q_i).Q_i, \qquad \omega_{i+1}^p = L^p(Q_{i+1}).Q_{i+1},$$
$$\phi_i^p = L^p(Q_i).f(Q_i), \qquad \phi_{i+1}^p = L^p(Q_{i+1}).f(Q_{i+1}),$$

for $p = 1, \ldots, 3$. We denote the characteristic velocities by $\lambda_L^p = \lambda^p(Q_i)$, $\lambda_R^p = \lambda^p(Q_{i+1})$, $p = 1, \ldots, 3$.

(2) Find out if there is a compressible sonic point across cell interface (i.e., if $\lambda_L > 0$ and $\lambda_R < 0$).

(3) **If** there is no sonic point, then we use upwinding to compute the numerical characteristic fluxes

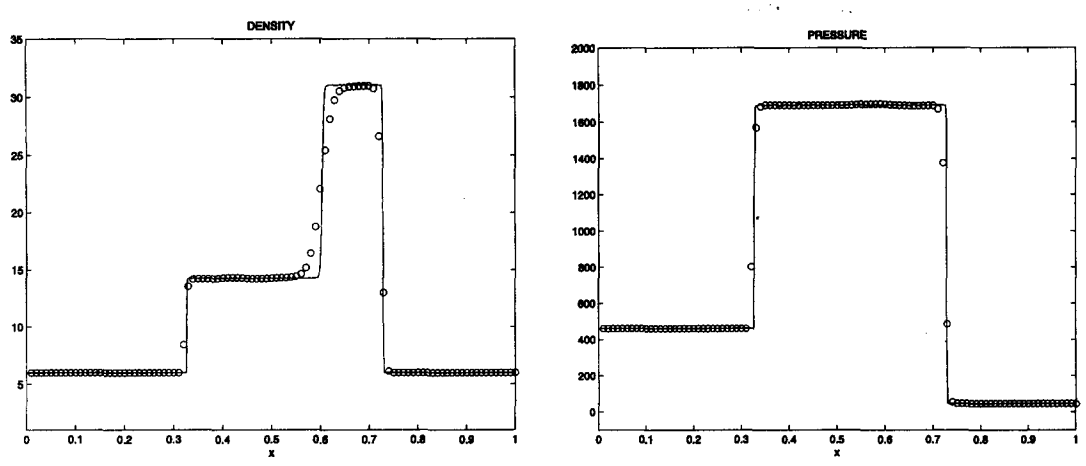

(a) Density. (b) Pressure.

Figure 11. Test example #1.

if $\lambda_L^k > 0$ and $\lambda_R^k > 0$, then $\phi_-^k = 0, \quad \phi_+^k = \phi_i^k$
if $\lambda_L^k < 0$ and $\lambda_R^k < 0$, then $\phi_-^k = \phi_{i+1}^k, \quad \phi_+^k = 0$

Else We consider an intermediate state and split the corresponding flux into a right and a left going portion, that is

$$\phi_-^k = \frac{\lambda_i^k \left(-\phi_{i+1}^k + \lambda_{i+1}^k \omega_{i+1}^k\right)}{\lambda_{i+1}^k - \lambda_i^k}, \tag{13}$$

$$\phi_+^k = \frac{\lambda_{i+1}^k \left(\phi_i^k - \lambda_i^k \omega_i^k\right)}{\lambda_{i+1}^k - \lambda_i^k}, \tag{14}$$

where

$$\lambda_{i+1}^k = \max\left(\left|\lambda_L^1\right|, \left|\lambda_L^3\right|, \left|\lambda_R^1\right|, \left|\lambda_R^3\right|\right), \tag{15}$$

and

$$\lambda_i^k = -\lambda_{i+1}^k, \tag{16}$$

for $k = 1, 2, 3$.

The numerical flux function is

$$F_{j+1/2}^n := F(Q_i, Q_{i+1}) = F^+ + F^- \tag{17}$$

$$= \sum_{p=1}^{3} \phi_+^p R^p(Q_i) + \sum_{p=1}^{3} \phi_-^p R^p(Q_{i+1}). \tag{18}$$

The first-order accurate scheme has the conservative form

$$Q_i^{n+1} = Q_i^n - \frac{\Delta t}{\Delta x}\left(F_{i+1/2}^n - F_{i-1/2}^n\right)$$

to assure that the shock is captured. The resulting scheme is a characteristic-based scheme, following the philosophy of Marquina's scheme [11], that avoids the use of averaged intermediate states and uses the transformation to the local characteristic fields, that correspond to local propagation independent waves.

We have implemented the scheme with PHM reconstruction of the characteristic fluxes in space, since as we have observed early, such procedure introduces an adequate numerical viscosity, and the TVD Shu-Osher Runge-Kutta methods for the time evolution [12].

We observe that the scheme works well, and the postshock oscillations are damped out to the same level of first-order accurate schemes. In Figure 10, we present numerical orbit for the

new scheme. This can be compared to Figures 6c′–e′ to see that the intermediate states deviate from the shock curve, and give a spiral form at the left states which resemble what we have observed with Marquina's, VL, SW schemes. The scheme gives interesting features. First, the intermediate states tend to return to Hugoniot, which might be related to the larger damping of the postshock errors observed in Figure 8. Another observation is that the left part of the present orbit moves closer to Hugoniot. We observe also the unsteady nature of the momentum peak value and the absence of postshock oscillations, which confirm what we have observed in Section 3 with the van Leer scheme. More numerical experiments on this numerical flux function are under investigation [17].

REMARK 3. The present flux function corrects the lack of dissipation of the SW-FVS by introducing the more diffusive HLL constructed in [16] in the neighborhood of the sonic points. It may be considered as a nonlinear way to dosify the viscosity of the HLL scheme using the sided characteristic fields.

5.3. Other Computational Difficulties and Numerical Tests

Most Godunov-type methods and other shock capturing schemes can display pathological behavior in certain flow situations [5,18], which includes the wall overheating, low density and internal energy flows, and the sonic point glitch, etc. We shall address mediated the improved flux function the linear and nonlinear waves, and show that the modified numerical scheme cannot only dissipate the postshock oscillations in slow-moving shocks, but also give good compromise between low noise and narrow shock profile and handles these other computational difficulties remarkably well.

TEST EXAMPLE #1. This flow problem is taken from [19], to test the robustness and accuracy of numerical methods. The solution contains four states separated by a left shock wave moving slowly to the left, a contact wave, and a strong shock wave traveling to the right. The results of the scheme equipped with the PHM reconstruction are shown in Figure 11. The three waves are well resolved and the scheme converges to the entropy solution. The new third-order scheme gives good results and shows an acceptable compromise between the low frequency noise and narrow shock and contact layers.

TEST EXAMPLE #2. WALL OVERHEATING. In this example, we consider the problem of a strong shock reflection from a rigid wall in one dimension gas. The initial conditions consist of a gas of constant density and pressure moving towards $x = 0$ in the domain $[0, 1]$; i.e.,

$$(p(x), u(x), e(x)) = (1, -1, 4), \qquad 0 < x < 1. \tag{19}$$

The boundary at $x = 0$ is a solid wall.

The "overheating effect" occurs in the first few zones near the wall, when the shock reflects off the stationary solid wall at the boundary. The overheating in the specific internal energy profile (peak) and the corresponding dip in the density are conspicuous, while the pressure and velocity have correct values.

Following Noh [14], this error is inevitable for any shock capturing method unsuccessful to model the heat conduction present in real fluids. He showed that a numerical scheme with a built-in heat conduction will be able to dissipate the overheating; i.e., the solution converges in the L^∞ sense.

Figure 12 shows numerical approximations obtained by the first- and third-order schemes. Although we observe a dip in the density (whose values are around 2% for the first-order scheme and 1.5% for the PHM scheme), this behavior is by no means extreme as the one observed in other experiments, e.g., [5,20]. The results show that the present scheme is able to reduce the "wall heating error" in the shock reflection problem.

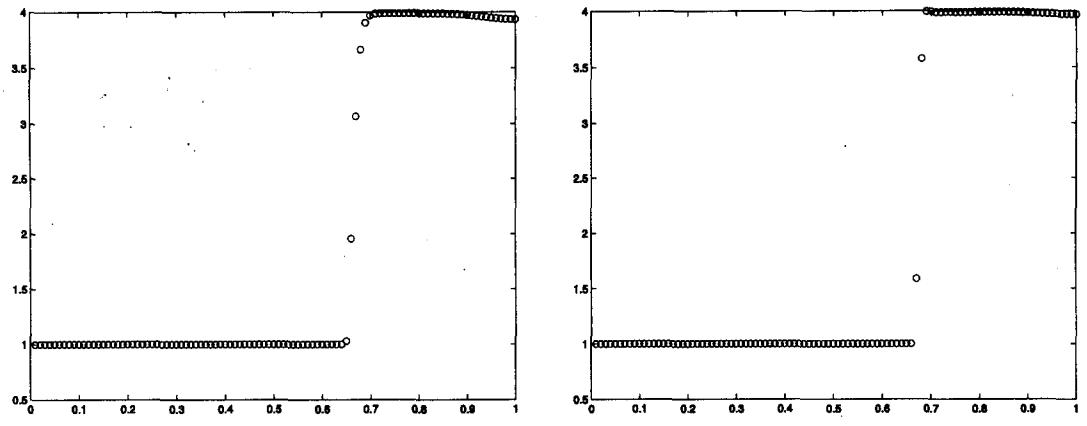

(a) First-order scheme. (b) Third-order scheme.

Figure 12. Shock reflection problem.

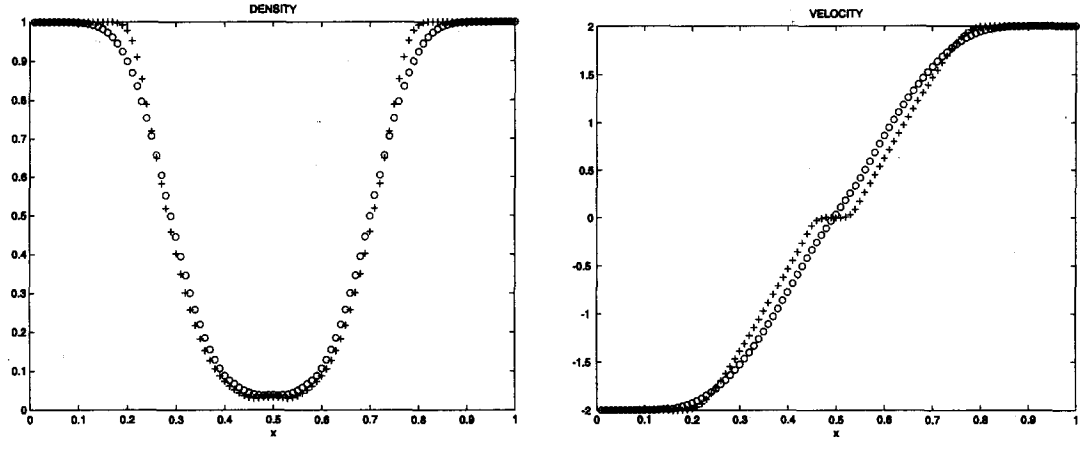

(a) Density. (b) Velocity.

Figure 13. Low density problem. (o): first-order, (+): third-order schemes.

TEST EXAMPLE #3. LOW DENSITY AND INTERNAL ENERGY FLOWS. Initial data are [11,21]

$$\begin{pmatrix} \rho \\ u \\ P \end{pmatrix} = \begin{cases} (1,-2,1)^\top, & x < 0.5, \\ (1,2,1)^\top, & x > 0.5. \end{cases}$$

The vacuum problem is a nonlinearizable Riemann problem where two rarefaction waves are formed and moving away from each other. These states are kinetic-energy rich which cause instabilities for shock capturing schemes [21]. Figure 13 displays the numerical results, where the first-order methods give similar results seen in [19] for HLL, SW, VL, and in [11] for Marquina's scheme. The third-order scheme of many FVS and FDS blow up early in the first time steps, because the density and internal energy become negative near the vacuum. However, our third-order scheme preserves positivity and gives good resolution.

TEST EXAMPLE #4. THE SONIC POINT GLITCH. In this example, we consider the problem from [19] with initial data

$$\begin{pmatrix} \rho \\ u \\ P \end{pmatrix} = \begin{cases} (1,0.75,1)^\top, & x < 0.3, \\ (0.125,0,0.1)^\top, & x > 0.3. \end{cases}$$

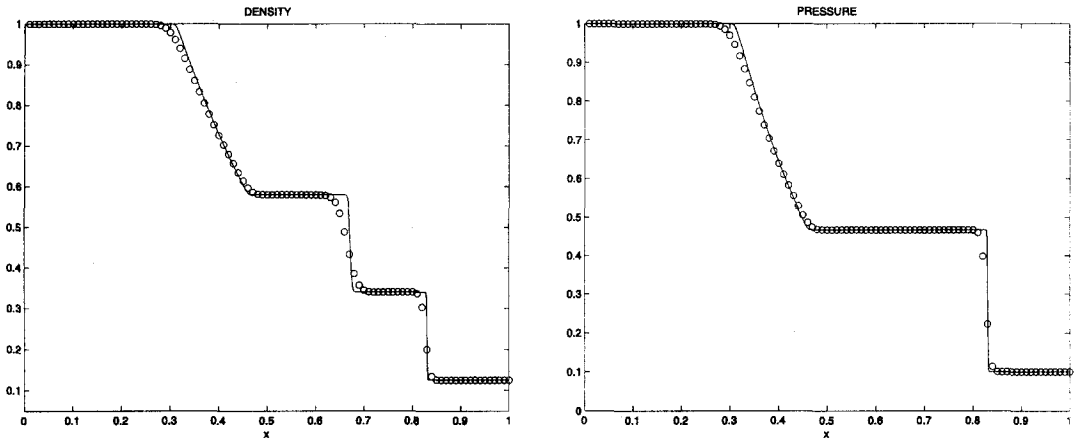

(a) Density. (b) Pressure.

Figure 14. Sonic glitch Riemann problem.

Figure 14 shows the profile of density and pressure with the first- and third-order schemes, at time $t = 2$ on a 100 zone grid. The results of the first-order scheme, not shown here, show a smaller $O(\Delta x)$ kink in the rarefaction wave region identical to that of many numerical schemes (see [19]). Such a glitch, also called "dogleg" phenomenon, is associated with the fact that at the point where the "glitch" situates the flow is sonic, hence, the velocity for the genuinely nonlinear wave field in zero [22]. Figure 14 shows the solution computed by the third-order PHM approximation where the sonic glitch disappears completely.

TEST EXAMPLE #5. A MACH 3 WIND TUNNEL WITH A STEP. This model problem was used by Colella and Woodward [23] to compare and test the performance of numerical methods. The setup of the problem is: the wind tunnel is 3 units long and 1 unit wide. The step is 0.2 units high and is located 0.6 units from the left-hand side of the tunnel. Inflow/outflow boundary conditions are applied at the left/right end of the computational domain, and reflective boundary conditions are applied along the wall of the tunnel. The problem is initialized by a right-going Mach 3 flow. The density profile is the hardest to compute due to numerical errors generated at the corner of the step (a singular point of the flow), along the upper wall at the contact discontinuity, and at reflecting boundaries. We treat it the same way as in [11]. Figure 15 shows the density contours at time $t = 4$. We can see that the shocks are well captured and accurate. The overheating errors are reduced (the level curves near the wall are more orthogonal). The "kinked" Mach steam and the numerical noise related to the "carbuncle phenomena" (associated to nearly stationary shocks near the reflecting wall) are reduced.

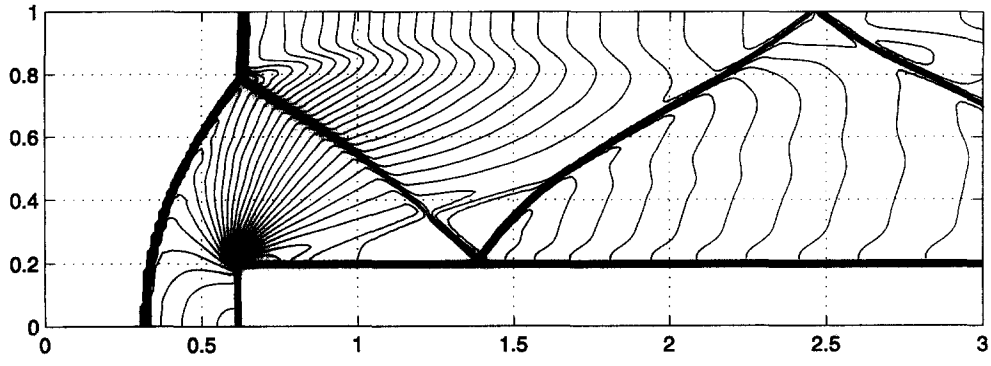

Figure 15. Mach 3 step flow problem. Contour plots of numerical approximations to the density by the third-order hyperbolic extension.

TEST EXAMPLE #6. DOUBLE MACH REFLECTION. This flow problem is also taken from [23]. The test involves a Mach 10 shock in air, $\gamma = 1.4$, initially making a 60 degree angle with the x-axis. The undisturbed air ahead of the shock has a density of 1.4 and pressure 1. We use the same boundary conditions of [23]. Figure 16 shows the equally spaced 30 density contours between the maximum and minimum values in $[0, 3] \times [0, 1]$. We can see that the second Mach is well computed. The jet, formed when the flow of the denser fluid is deflected by a pressure gradient in the region when the first contact discontinuity approaches the reflected wall, is well captured. The curved reflected shock is moving rapidly at its right end and is not moving at all at its left end, which presents a computational difficulty for many finite difference schemes [24]. Our schemes give good results without oscillations.

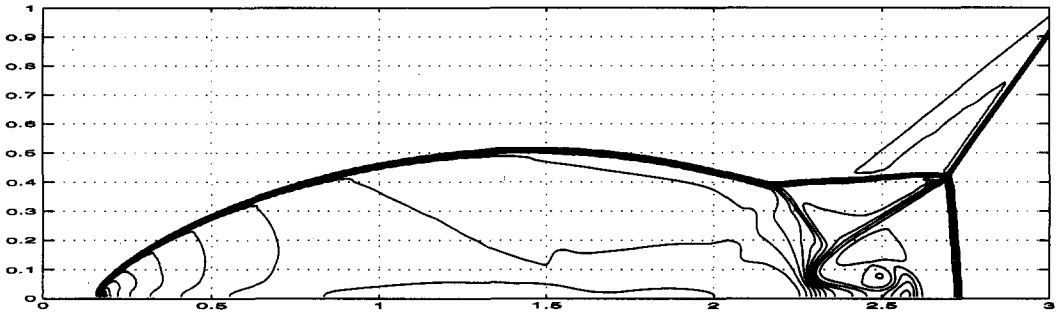

Figure 16. Double Mach reflection problem. Contour plots of numerical approximations to the density by the third-order hyperbolic extension.

6. CONCLUSION

A careful comparison of different numerical schemes in conservation form in slowly moving shock computations allows us to establish that the observed postshock errors are not restricted to a particular kind of scheme; all the schemes suffer from these disturbances. The error has a local character; it appears in the first steps when the solution changes from an artificially narrow to a continuous profile. The noise perturbs largely the viscous profile and begins to propagate from the shock position. In some schemes, the error seems to be continuously generated and propagates away from the shock location as a wavy tail. In other schemes the generation of postshock errors seems to be reduced to computationally acceptable levels after a discrete smooth transition between the left and right states has been achieved.

We have considered two essentially different reconstruction procedures to construct higher-order versions of the basic first-order schemes we have considered. We have observed that with the piecewise polynomial reconstruction, the numerical noise is preserved further upstream than with the piecewise hyperbolic reconstruction.

The study of the internal shock structure and the behavior of the intermediate states lead us to design a parameter-free entropy-fix type scheme that completely dissipates the oscillations, in its first-order versions as well as in its PHM-based third-order extension. The new scheme gives good compromise between low noise and narrow shock profile and fixes or reduces a variety of numerical pathologies, like the overheating errors, the sonic point glitch, and the low density flow.

REFERENCES

1. M. Arora and P. Roe, On post-shock oscillations due to shock capturing schemes in unsteady flow, *J. Comput. Phys.* **130**, 1–24, (1997).
2. S. Jin and J. Liu, The effects of numerical viscosity I: Slowly moving shock, *J. Comput. Phys.* **126**, 373–389, (1996).
3. S. Karni and S. Canic, Computations of slowly moving shocks, *J. Comput. Phys.* **136**, 132–139, (1997).
4. H.C. Lin, Dissipation additions to flux-difference splitting, *J. Comput. Phys.* **117**, 20–27, (1995).

5. J.J. Quirk, A contribution to the great Riemann debate, *Internat. J. Numer. Methods Fluids* **18**, 555–574, (1994).
6. T.W. Roberts, The behavior of flux difference splitting schemes near slowly moving shock waves, *J. Comput. Phys.* **90**, 141–160, (1990).
7. P. Colella and P. Woodward, The piecewise-parabolic method (PPM) for gas-dynamic simulations, *J. Comput. Phys.* **54**, 174–201, (1984).
8. J.L. Steger and R.F. Warming, Flux-vector splitting of the inviscid gas dynamic equations with applications to finite-difference methods, *J. Comput. Phys.* **40**, 489–500, (1981).
9. B. van Leer, *Flux-Vector Splitting for the Euler Equations*, Lecture Notes in Physics, Springer-Verlag, (1982).
10. P.L. Roe, Approximate Riemann solvers, parameter vectors, and difference schemes, *J. Comput. Phys.* **43**, 357–372, (1981).
11. R. Donat and A. Marquina, Capturing shock reflections: An improved flux formula, *J. Comput. Phys.* **125**, 42–58, (1996).
12. C.W. Shu and S. Osher, Efficient implementation of essentially non-oscillatory shock capturing schemes (two), *J. Comput. Phys.* **83**, 32–78, (1989).
13. A. Marquina, Local piecewise hyperbolic reconstruction of numerical fluxes for nonlinear scalar conservation laws, *SIAM J. Sci. Comput.* **15**, 892, (1994).
14. W. Noh, Errors for calculations of strong shocks using an artificial heat flux, *J. Comput. Phys.* **72**, 78–120, (1987).
15. Y. Stiriba, Ph.D. Thesis, GrAN Report n. 00-03, `http://gata.uv.es/eng/reports.html`.
16. A. Harten, P.D. Lax and B. van Leer, On upstream differencing and Godunov-type schemes for hyperbolic conservation laws, *SIAM Review* **23**, 35–61, (1983).
17. Y. Stiriba, Non-linear flux split method for hyperbolic conservation laws, *J. Comput. Phys.* **176**, 20–39, (2002).
18. R.J. LeVeque, Nonlinear conservation laws and finite volume methods for astrophysical fluid flow, In *Comp. Methods for Astrophysical Fluid Flow*, (Edited by O. Steiner and A. Gautschy), Springer-Verlag, (1998).
19. E.F. Toro, *Riemann Solvers and Numerical Methods for Fluid Dynamics*, Second Edition, Springer-Verlag, (1999).
20. P. Glaister, An approximate linearized Riemann solver for the Euler equations for real gases, *J. Comput. Phys.* **74**, 382–408, (1988).
21. B. Einfeldt, C.D. Munz, P.L. Roe and B. Sjogreen, On Godunov-type methods near low densities, *J. Comput. Phys.* **92**, 273–295, (1991).
22. K. Xu and H.-Z. Tang, An explanation for the sonic point glitch, `http://www.math.ntnu.no/conservation/2000/011.html`.
23. P. Woodward and P. Colella, The numerical simulation of two-dimensional fluid flow with strong shocks, *J. Comput. Phys.* **54**, 115–173, (1984).
24. S. Jin and Z.P. Xin, The relaxation schemes for systems of conservation laws in arbitrary space dimensions, *Comm. Pure. Appl. Math.* **48**, 235–276, (1995).